Simultaneous X-ray Nano-Ptychographic and Fluorescence Microscopy at the Bionanoprobe

S. Chen*[a], J. Deng[b], D. J. Vine[a], Y. S. G. Nashed[c], Q. Jin[d], T. Peterka[c], C. Jacobsen[a,b,d,e], S. Vogt[a]

[a]X-ray Science Division, Advanced Photon Source, Argonne National Laboratory, Argonne, IL 60439, USA; [b]Applied Physics, Northwestern Univ., Evanston, IL 60208, USA; [c]Mathematics and Computing Science Division, Argonne National Laboratory, Argonne, IL 60439, USA; [d]Dept. of Physics and Astronomy, Northwestern Univ., Evanston, IL 60208, USA; [e]Chemistry of Life Processes Institute, Northwestern Univ., Evanston, IL 60208, USA

ABSTRACT

Hard X-ray fluorescence (XRF) microscopy offers unparalleled sensitivity for quantitative analysis of most of the trace elements in biological samples, such as Fe, Cu, and Zn. These trace elements play critical roles in many biological processes. With the advanced nano-focusing optics, nowadays hard X-rays can be focused down to 30 nm or below and can probe trace elements within subcellular compartments. However, XRF imaging does not usually reveal much information on ultrastructure, because the main constituents of biomaterials, i.e. H, C, N, and O, have no fluorescence lines (H) or low fluorescence yield (C, N and O) and little absorption contrast at multi-keV X-ray energies. An alternative technique for imaging ultrastructure is ptychography. One can record far-field diffraction patterns from a coherently illuminated sample, and then reconstruct the complex transmission function of the sample. In theory the spatial resolution of ptychography can reach the wavelength limit. In this manuscript, we will describe the implementation of ptychography at the Bionanoprobe (a recently developed hard XRF nanoprobe at the Advanced Photon Source) and demonstrate simultaneous ptychographic and XRF imaging of frozen-hydrated biological whole cells. This method allows locating trace elements within the subcellular structures of biological samples with high spatial resolution. Additionally, both ptychographic and XRF imaging are compatible with tomographic approach for 3D visualization.

Keywords: hard X-ray fluorescence microscopy, ptychography, 3D

1. INTRODUCTION

Trace elements, particularly metals such as Fe, Cu, and Zn, play important roles in many biological processes. Synchrotron-based hard X-ray fluorescence (XRF) microscopy offers unparalleled sensitivity to quantitatively study these trace elements in biological samples with a sub-micron spatial resolution [1]. Many-micron-thick biological samples, such as thick tissues and whole cells, can be imaged without sectioning due to non-destructive nature of X-ray photons and high penetration capability of hard X-rays.

Recently, we installed an XRF nanoprobe, named Bionanoprobe (BNP), at an undulator beamline at the Advanced Photon Source (APS) of Argonne National Laboratory (ANL), dedicated for high-resolution (sub-100 nm) studies [2]. In addition to high spatial resolution, the BNP also enables cryogenic experiments. Biological samples can be directly examined in their frozen-hydrated state, with 3D structures and elemental compositions much better preserved compared to dehydrated structures [3,4,5,6] and significantly higher radiation resistance compared to wet samples being examined at the room temperature [7,8]. By using the BNP, we are able to learn about the subcellular structures based on the trace elemental maps to some extend. For example, the cell volume is often outlined by fairly uniform S distribution with P and Zn content elevated in the nucleus region and Mn concentrated in mitochondria. However, a comprehensive understanding of ultrastructure is very challenging. Both the XRF and transmission imaging are nearly blind to the main constituents of biological samples, i.e. H, C, N, and O, mainly due to their low fluorescence yield [9] and little absorption contrast at multi-keV X-ray energies.

An alternative technique for imaging the ultrastructure of biological samples is ptychography, a coherent diffraction imaging (CDI) method. It has been successfully demonstrated on imaging diatoms [10], bacteria [11] and yeast cells [12]. Ptychographic imaging yields reconstructed phase images of a sample with enhanced phase contrast and higher

*sichen@anp.anl.gov; phone 1 630 252-0807; www.aps.anl.gov

spatial resolution. We have implemented ptychography at the BNP, and performed ptychographic imaging at the same time of XRF mapping [13]. By combining these two complementary imaging modes, it is straightforward to correlate the elemental compositions with the ultrastructure of an object. Additionally, both ptychographic and XRF imaging are compatible with tomographic approach for 3D visualization. In this manuscript, we describe the implementation of ptychography at BNP and demonstrate simultaneous ptychographic and XRF imaging of a frozen-hydrated biological whole cell.

2. EXPERIMENTAL SETUP

The BNP was installed at an undulator beamline of the Life Sciences Collaboration Team (LS-CAT) at the APS. This beamline delivers 4.5 - 35 keV X-ray photons. White beam slits and a double-crystal Si <111> monochromator were installed at ~27 m and 60 m from the undulator source, respectively. The BNP is at ~5 m downstream of the monochromator with a vacuum chamber (10^{-7}-10^{-8} Torr) housing mainly X-ray optics, a sample stage assembly, a sample-changing robot, and several detectors. Eight Fresnel zone plates were installed as nano-focusing optics, allowing fast switching for different spatial resolutions and incident X-ray energy settings. While the sample is raster scanned through the focal spot, a full XRF spectrum is recorded at each step using a silicon drift detector (Vortex-ME4) mounted at 90° with regards to the incident beam. For ptychographic imaging, a pixelated area detector (Dectris Pilatus 100K) positioned at ~2.2 m downstream from the BNP (measured from the sample position) is used to record a diffraction pattern at each scanning step. The diffraction patterns are then used to reconstruct the complex transmission function of the object via the extended ptychographic iterative engine (ePIE) algorithm [14]. Note that significant oversampling is required to ensure the success of reconstruction. To minimize signal attenuation by the ambient air, a tube filled by He gas is placed between the downstream end of the BNP and the area detector. A schematic of the experimental setup is shown in Figure 1.
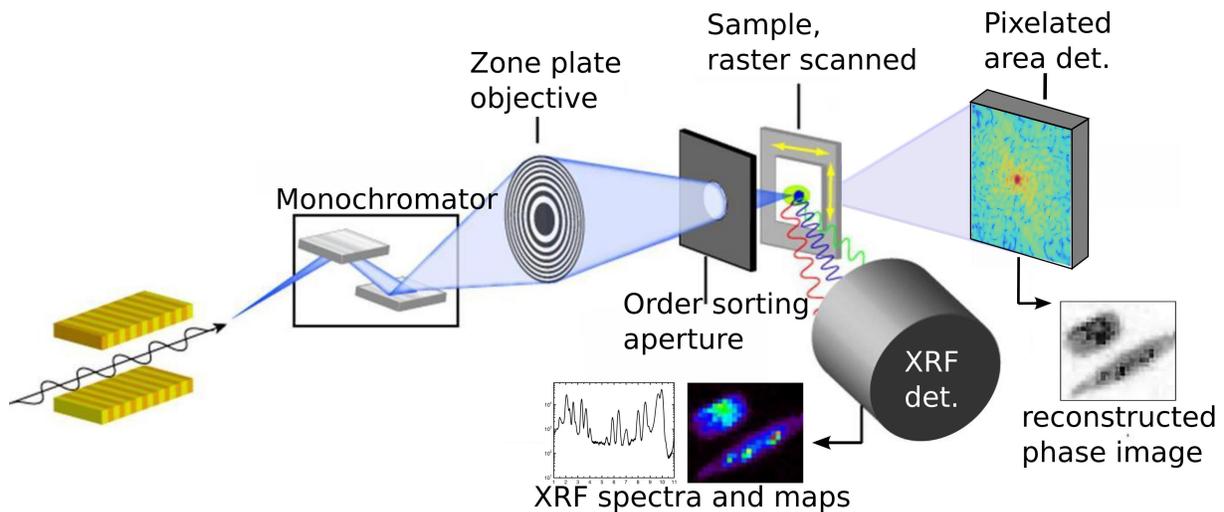

Figure 1. Schematic showing the experimental setup for simultaneous fluorescence and ptychographic imaging (not to scale). A monochromatized X-ray beam is focused onto the sample using a Fresnel zone plate. While the sample is raster scanned, XRF spectra and far-field diffraction patterns are recorded, respectively, using a fluorescence detector mounted at 90° with regards to the incident beam and a pixelated area detector mounted at ~2.2m downstream of the sample.

To evaluate the setup, an Au test pattern was imaged using a zone plate with 70 nm outmost zone width and 160 μm diameter (ZP70-160) at 10 keV incident energy. While the coherence degree of incident beam, particularly in the longitudinal direction, can be increased by reducing the white beam slits opening, the balance between the coherence degree and total X-ray beam flux must be considered. We chose to use 30-40 μm opening for the horizontal white beam

slits, which delivers higher flux at the cost of longitudinal coherence degree. Accordingly, we applied several mutually incoherent probe modes in the reconstruction algorithm [15]. Figure 2 shows both the reconstructed ptychographic image and Au XRF map of spoke structures on the test pattern. A significant improvement in the spatial resolution is observed in the image acquired using ptychography. While the spatial resolution of XRF imaging is limited by the Raleigh resolution of the optics (84 nm for ZP70-160), ptychographic imaging is, in theory, only limited by the wavelength of incident photons.
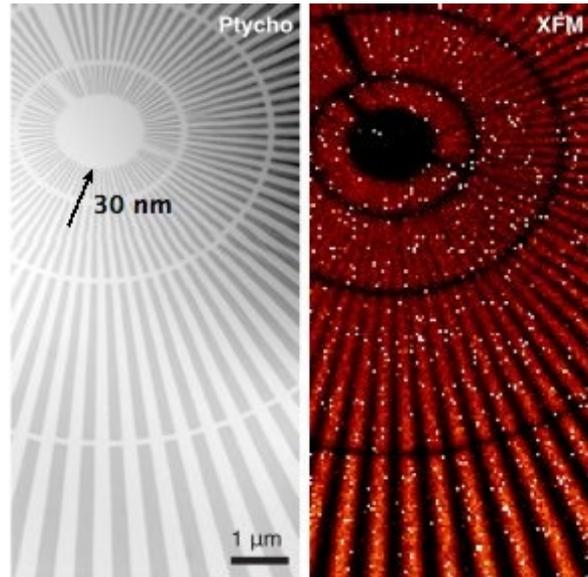

Figure 2. The reconstructed ptychographic image and Au XRF map of spoke structures on an Au test pattern. The images were obtained by performing a scan of 100 steps in the horizontal direction and 200 steps in the vertical direction with 50 nm step size and 50 ms dwell time per step. (a) Reconstructed phase image via ptychography, where the 30 nm inner spokes can be clearly visualized. The reconstruction was carried out using ePIE algorithm. (b) Au XRF map, where the central spokes are not distinguishable.

3. IMAGING OF FROZEN-HYDRATED BIOGICAL SAMPLES

One of the challenges of imaging biological samples using either X-ray or electron probe, particularly for high-resolution imaging, is radiation damage [16,17,18,19]. The radiation tolerance of biological samples can be greatly improved by maintaining them in their frozen-hydrated state and imaging them in cryogenic conditions [7,8]. In addition, both the structures and ionic elemental compositions are preserved with higher fidelity in frozen-hydrated samples compared to samples prepared using dehydration methods [3,4,5,6]. As a demonstration, we imaged a frozen-hydrated unicellular green algae (*Chlamydomonas reinhardtii*) cell at ~130 K using simultaneous XRF and ptychography at the BNP. The sample was plunge frozen and then directly transferred into the BNP chamber using a liquid-nitrogen-cooled sample transfer chamber. We used 5.2 keV incident X-ray beam in order to maximize the partially coherent flux and image contrast for biological samples.

Figure 3 shows both the ptychographic image of the algae cell and the XRF maps of S, K and Ca. Very detailed membrane and subcellular structures are revealed via ptychography approach. A few of the electron-dense spherical structures are high in Ca, which are presumably polyphosphate bodies containing polyphosphate complexed with Ca [20]. As indicated by the arrows in the images, the pyrenoid in the chloroplast is identified by both the phase contrast in the ptychographic image and the slightly elevated S concentration in the XRF image. Note that K, one of the most diffusible ions in the cell and often lost during traditional sample preparation using chemical fixatives, was well preserved by using the cryogenic method.
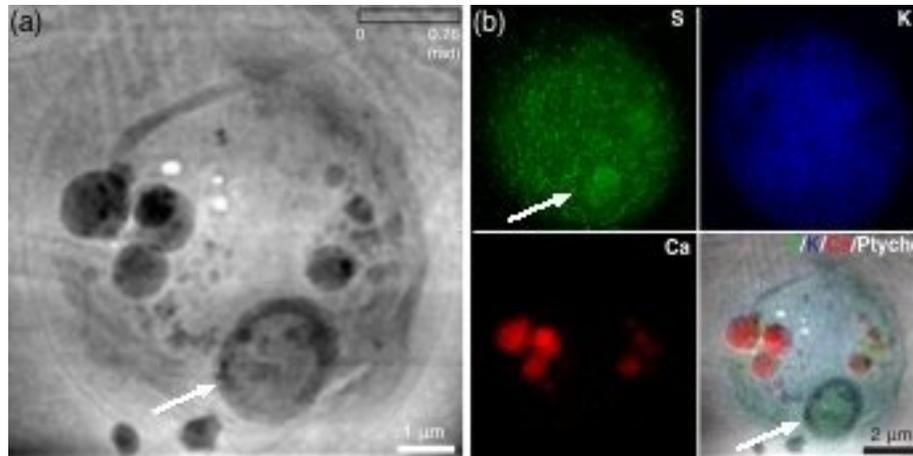
Figure 3. Reconstructed ptychographic image and XRF maps of a frozen-hydrated unicellular green algae (*Chlamydomonas reinhardtii*) cell. The images were obtained by performing a scan of 167 steps in the horizontal direction and 151 steps in the vertical direction. (a) Reconstructed phase image of the cell via ptychography showing detailed membrane and subcellular structures. The reconstruction was carried out using ePIE algorithm with two probe modes. (b) XRF maps of S, K, Ca, and the overlay of the elements and the reconstructed phase image. This figure was adapted from Fig.4 in [13].

4.   3D IMAGING

Both ptychographic and fluorescence imaging are compatible with tomographic approach for non-destructive 3D visualization. However, obtaining large datasets with high spatial resolution is challenging due to the limited beamtime. One solution is to speed up data acquisition, for example, by using fly-scan, i.e. continuous motion for the inner loop of a scan, as oppose to step-scan. While fly-scan has been routinely used for fluorescence microscopy, difficulties arise for ptychographic imaging. The diffraction patterns are blurred by a continuously moving sample, which adds complexity to reconstruction. To address this issue, we again applied multiple probe modes [15], which was used to compensate for incoherent illumination, and successfully demonstrated fly-scan ptychography at the BNP [21]. Figure 4 shows a reconstructed 3D image of a 200 nm thick test structure on the Au test pattern. A total of 31 projections were obtained with 4° rotation step. Each ptychographic projection was obtained using fly-scan mode with 100 ms dwell time per pixel and then reconstructed independently using ePIE with five probe modes.

Figure 4. Reconstructed 3D ptychographic image of "20" on an Au test pattern. A total of 31 projections were obtained with 4° rotation step. Each projection was acquired by performing a fly scan, then reconstructed using ePIE with five probe modes [22].

5. SUMMARY

We have implemented ptychographic imaging at the BNP, a sample-scanning hard XRF nanoprobe, and demonstrated simultaneous ptychographic and XRF imaging of frozen-hydrated biological samples. This method enables two independent but complementary contrast modes at the same time: XRF imaging at the BNP quantitatively maps the distribution of elements with their atomic numbers equal or larger than 13 (Al), whereas ptychographic imaging yields structural information with higher spatial resolution, defined mostly by the lightest elements including H, C, N, and O in biological samples. Additionally, both of the techniques are extendable to 3D imaging, which have been demonstrated on a metallic test structure and will be applied on imaging of biological samples.

6. ACKNOWLEDGEMENT

REFERENCES

[1] Fahrni, C. J., "Biological applications of X-ray fluorescence microscopy: exploring the subcellular topography and speciation of transition metals," Curr Opin in Chem Biol 11, 121-7 (2007).

[2] Chen, S., Deng, J., Yuan, Y., Flachenecker, C., Mak, R., Hornberger, B., Jin, Q., Shu, D., Lai, B., Maser, J., Roehrig, C., Paunesku, T., Gleber, S., Vine, D. J., Finney, L., VonOsinski, J., Bolbat, M., Spink, I., Chen, Z., Steel, J., Trapp, D., Irwin, J., Feser, M., Snyder, E., Brister, K., Jacobsen, C., Woloschak, G. and Vogt, S., "The Bionanoprobe: hard X-ray fluorescence nanoprobe with cryogenic capabilities," J Synchrotron Rad 21, 66-75 (2014).

[3] O'Toole, E., Wray, G., Kremer, J. and McIntosh, J. R., "High voltage cryomicroscopy of human blood platelets," J Struct Biol 110(1), 55-66 (1993).

[4] Williams, S., Zhang, X., Jacobsen, C., Kirz, J., Lindaas, S., Van't Hof, J. and Lamm, S. S., "Measurement of wet metaphase chromosomes in the scanning transmission X-ray microscope," J Microsc 170(2), 155-65 (1993).

[5] Vanhecke, D., Asano, S., Kochovski, Z., Fernandez-Busnadiego, R., Schrod, N., Baumeister, W. and Luceice, V., "Cryo-electron tomography: methodology development and biological applications," J Microsc 242(3), 221-7 (2010).

[6] Beveridge, T. J., "Bacterial cell wall structure and implications for interactions with metal ions and minerals," J Nucl Radiachem Sci 6, 7-10 (2005).

[7] Sayre, D. and Chapman, H. N., "X-ray microscopy," Acta Cryst A 51(3), 237-52, (1995).

[8] Maser, J., Osanna, A., Wang, Y., Jacobsen, C., Kirz, J., Spector, S., Winn, B. and Tennant, D. "Soft X-ray microscopy with a cryo scanning transmission X-ray microscope: I. instrumentation, imaging and spectroscopy," J Microsc 197, 68-79 (2000).

[9] Krause, M., "Atomic radiative and radiationless yields for K and L shells," J Phys Chem Ref Data 8(2), 307-27 (1979).

[10] Vine, D. J., Pelliccia, D., Holzner, C. , Baines, S. B., Berry, A., McNulty, I., Vogt, S., Peele, A. G. and Nugent, K., A., "Simultatneous X-ray fluorescence and ptychographic microscopy of Cyclotella meneghiniana," Opt Express 20(16), 18287-96 (2012).

[11] Wilke, R. N., Priebe, M., Bartels, M., Giewekemeyer, K., Diaz, A., Karvinen, P. and Saldit, T., "Hard X-ray imaging of bacterial cells: nano-diffraction and ptychographic reconstruction," Opt Express 20(17), 19232-54 (2012).

[12] Lima, E., Diaz, A., Guizar-Sicairos, M., Gorelick, S., Pernot, P., Schleier, T. and Menzel, A., "Cryo-scanning X-ray diffraction microscopy of frozen-hydrated yeast," J Microsc 249(1), 1-7 (2013)

[13] Deng, J., Vine, D. J., Chen, S., Nashed, Y. S. G., Jin, Q., Phillips, N. W., Peterka, T., Ross, B., Vogt, S. and Jacobsen, C., "Simultaneous cryo X-ray ptychographic and fluorescence microscopy of green algae," PNAS 112(8), 2314-2319 (2015).

[14] Maiden, A. M. and Rodenburg, J. M., "An improved ptychographical phase retrieval algorithm for diffractive imaging," Ultramicroscopy 109(10), 1256-62 (2009).

[15] Thibault, P. and Menzel, A., "Reconstructing state mixtures from diffraction measurements," Nature 494(7435), 68-71 (2013).

[16] Kirz, J., Jacobsen, C. and Howells, M., "Soft X-ray microscopes and their biological applications," Q Rev Biophys 28(1), 33-130 (1995).

[17] Beetz, T. and Jacobsen, C., "Soft X-ray radiation-damage studies in PMMA using a cryo-STXM," J Synchrotron Rad 10, 280-3 (2003).

[18] Nishino, Y., Takahashi, Y., Imamoto, N., Ishikawa, T. and Maeshima, K., "Three-dimensional visualization of a human chromosome using coherent X-ray diffraction," Phys Rev Lett 102, 018101 (2009).

[19] Howells, M., Beetz, T., Chapman, H. N., Cui, C., Holton, J. M., Jacobsen, C. J., Kirz, J., Lima, E., Marchesini, S., Miao, H., Sayre, D., Shapiro, D. A., Spence, J. C. H. and Starodub, D., "An assessment of resolution limitation due to radiation-damage in X-ray diffraction microscopy," J Electron Spectrosc. Relat. Phenom 170, 4-12 (2009).

[20] Komine, Y., Eggink, L. L., Park, H. and Hoober, J. K., "Vacuolar granules in Chlamydomonas reinhardtii: polyphosphate and a 70-kDa polypeptide as major components," Planta 210(6), 897-905 (2000).

[21] Deng, J., Nashed, Y. S. G., Chen, S., Vine, D. J., Phillips, N. W., Peterka, T., Ross, B., Vogt, S., Jacobsen, C. and Vine, D. J., "Continuous motion scan ptychography: characterization for increased speed in coherent X-ray imaging," Opt Express 23(5), 5438-51(2015).

[22] Deng, J., Vine, D. J., Chen, S., Nashed, Y. S. G, Jin, Q., Peterka, T., Vogt, S. and Jacobsen, C., "Advances and challenges in high-resolution & high-throughput ptychography," submitted.